

Fermi-surface topology of the iron pnictide LaFe_2P_2

S. Blackburn,¹ B. Prévost,¹ M. Bartkowiak,^{2,*} O. Ignatchik,² A. Polyakov,² T. Förster,² M. Côté,¹ G. Seyfarth,^{1,3,4} C. Capan,⁴ Z. Fisk,⁴ R. G. Goodrich,⁵ I. Sheikin,³ H. Rosner,⁶ A. D. Bianchi,¹ and J. Wosnitzer²

¹*Département de Physique and RQMP, Université de Montréal, Montréal H3C 3J7, Canada*

²*Hochfeld-Magnetlabor Dresden (HLD), Helmholtz-Zentrum Dresden-Rossendorf and TU Dresden, D-01314 Dresden, Germany*

³*Laboratoire National des Champs Magnétiques Intenses (LNCMI), CNRS, UJF, 38042 Grenoble, France*

⁴*Department of Physics and Astronomy, University of California Irvine, Irvine, California 92697, USA*

⁵*Department of Physics, George Washington University, Washington, DC, 20052, USA*

⁶*Max Planck Institute for Chemical Physics of Solids, 01187 Dresden, Germany*

(Dated: June 24, 2014)

We report on a comprehensive de Haas–van Alphen (dHvA) study of the iron pnictide LaFe_2P_2 . Our extensive density-functional band-structure calculations can well explain the measured angular-dependent dHvA frequencies. As salient feature, we observe only one quasi-two-dimensional Fermi-surface sheet, i.e., a hole-like Fermi-surface cylinder around Γ , essential for s_{\pm} pairing, is missing. In spite of considerable mass enhancements due to many-body effects, LaFe_2P_2 shows no superconductivity. This is likely caused by the absence of any nesting between electron and hole bands.

PACS numbers: 71.18.+y, 71.27.+a, 74.25.Jb

The very unique Fermi-surface topology of many iron-pnictide superconductors stimulated a number of theories on the nature of the pairing interactions in these materials. The degree of nesting between quasi-two-dimensional hole and electron bands is especially regarded as a key ingredient for a possible extended s -wave pairing mechanism [1–4]. Besides such intriguing topological nesting aspects of the Fermi surface, other scenarios start from a more localized picture to explain e.g. antiferromagnetism [5]. A dual description of both itinerant and localized degrees of freedom of the Fe d electrons is also considered [6, 7]. In the latter cases, strong electronic correlations are expected that lead to concomitant renormalized effective masses.

The precise knowledge of the electronic structure and many-body interactions, therefore, is a prerequisite for testing the above scenarios. The Fermi surface and band-resolved mass enhancement of metals can ideally be investigated by quantum-oscillation studies in combination with state-of-the-art band-structure calculations [8]. Indeed, such kind of investigations have been reported for a number of iron pnictides, including several members of the 122 family XFe_2As_2 ($X = \text{Ba}, \text{Sr}, \text{Ca}$) [9–11] (see Refs. 12, 13 for recent reviews). Important results on the topology of the Fermi surfaces and many-body mass enhancements have been obtained already, but more information is needed for gaining a coherent picture on the band-structure properties relevant for superconductivity in these materials.

Here, we report on a detailed de Haas–van Alphen (dHvA) study combined with band-structure calculations of the 122 iron phosphide LaFe_2P_2 . Replacing in CaFe_2As_2 the divalent Ca by trivalent rare earths of similar size leads, in the case of La-doped CaFe_2As_2 , to superconducting transition temperatures up to about 47 K and a concomitant re-arrangement of the electronic

structure which could be driven by the interlayer As–As p -orbital separation [14]. LaFe_2P_2 , however, is a nonsuperconducting analog of the iron-arsenide superconductors of the 122 family. LaFe_2P_2 is a Pauli-paramagnetic metal with trivalent non-magnetic rare-earth La atoms [15] showing no signs of any magnetic or superconducting order down to 20 mK. The electronic structure, though anisotropic, is rather three dimensional and characterized by a strongly corrugated quasi-two-dimensional electron Fermi-surface sheet, as well as a donut-shaped, and a strongly branched Fermi surface. Band-structure calculations describe well the experimentally determined dHvA frequencies.

High-quality single crystals of LaFe_2P_2 were grown from excess Sn flux [16]. The sample used for our experiments has dimensions of $0.15 \times 0.1 \times 0.05 \text{ mm}^3$. We measured dHvA oscillations by use of capacitive cantilever torque magnetometers, that could be rotated *in situ* around one axis. The torque, $\vec{\tau} = \vec{M} \times \vec{B}$, results from the interaction between the non-uniform magnetization \vec{M} of the sample with the applied magnetic field \vec{B} . The measurements were performed both at the Dresden High Magnetic Field Laboratory (HLD) using a superconducting 20-T magnet and at the Grenoble High Magnetic Field Laboratory (LNCMI-Grenoble) using a resistive water-cooled magnet reaching 34 T. The cantilevers were mounted in both places directly in the $^3\text{He}/^4\text{He}$ mixtures of top-loading dilution refrigerators placed inside the magnets.

Since the resulting Fermi-surface topology is very sensitive to details of the chosen approximations [17], we used two different methods to calculate the electronic band structure. Indeed, as seen below, both methods give somewhat different dHvA frequencies, although the main features of the Fermi-surface topology are nicely reproduced in both calculations. Using these two dif-

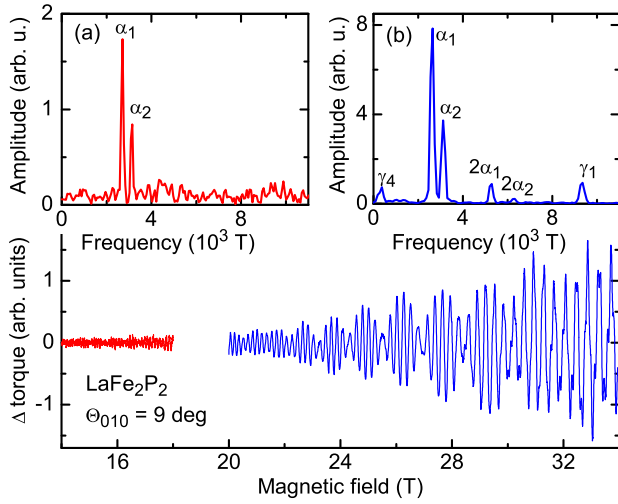


FIG. 1: (Color online) The main panel shows the background-subtracted torque signal obtained at about 30 mK in a superconducting magnet from 14 to 18 T at the HLD and in a resistive magnet between 20 and 34 T at the LNCMI-Grenoble. The fields were aligned by about 9° from the c towards the a axis. The inset (a) shows the Fourier transformation of the HLD data, the inset (b) that of the Grenoble data.

ferent methods allowed us to get a better insight in the reliability and the error bars of the extracted extremal orbits. First, we applied the full-potential local-orbital (FPLO) code [18] on a $24 \times 24 \times 24$ k mesh. Exchange and correlation potentials were estimated using the local density approximation (LDA) [19]. Very similar results were obtained when using the generalized gradient approximation (GGA) [20]. For these calculations, we used the structural data of Ref. 16, but we allowed the P atoms to relax their z position [21]. Since it is known that in LDA $4f$ states tend to shift too close to the Fermi energy [22], in a next step we forced the La $4f$ states away from the Fermi energy by adding the Coulomb correlation energy, expressed by U [23]. This LDA+ U formalism led only to minor changes in the band structure.

Further, the band structure was calculated through density functional theory using the ABINIT code [24] with the projector-augmented wave formalism using the GGA [20]. The wave functions were calculated on a $16 \times 16 \times 16$ k -point grid in the first Brillouin zone using a plane-wave basis up to an energy cutoff of 40 Ha (1088 eV). Here, the P atom positions were relaxed as well. We used the experimentally determined distance between the FeP planes in our calculations.

In our sample, we were able to resolve dHvA oscillations starting at about 10 T on top of smoothly varying background torque signals. We observed dHvA oscillations for all orientations of the applied magnetic field. Seven independent dHvA frequencies could be resolved over the whole angular range. In earlier measurements, only three frequencies occurring over a restricted angular

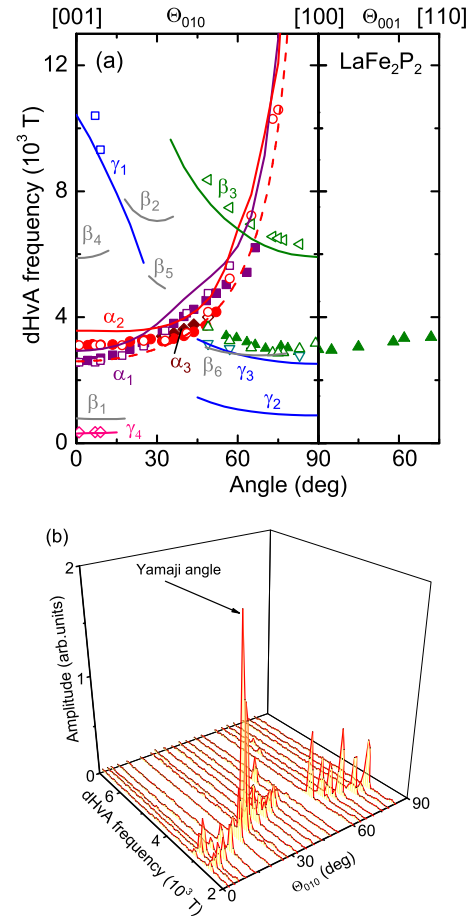


FIG. 2: (Color online) (a) Angular dependence of the dHvA frequencies. Closed (open) symbols are experimental values obtained at the HLD (LNCMI-Grenoble), while solid lines correspond to the calculated extremal Fermi-surface orbits using the ABINIT code. The α orbits come from the electron-like cylinder at X , the γ orbits from the donut, and the β orbit from the multi-branched Fermi surface (Fig. 3) (see main text for details). The dashed curve shows a $1/\cos(\Theta)$ dependence expected for a cylindrical Fermi surface. (b) 3D plot of the Fourier spectra obtained for the field window between 14 and 18 T. The α_1 and α_2 orbits merge at the Yamaji angle of about 25° where the dHvA amplitude peaks clearly.

range were reported for LaFe_2P_2 [25]. Typical examples of background-subtracted (using fourth-order polynomials) dHvA torque signals are shown in the main panel of Fig. 1. For this field orientation – the magnetic field was rotated by about 9° from the c towards the a axis – data up to 18 T taken at the HLD in Dresden and from 20 up to 34 T obtained in Grenoble are available [26]. A beating of the oscillating signal is evident which reflects the existence of two slightly different dHvA frequencies. This is quantified by the Fourier transformations of the signals. For the low-field data [Fig. 1(a)], only the two beating frequencies at $F_{\alpha_1} = 2640(30)$ T and $F_{\alpha_2} = 3120(30)$ T could be resolved, while in the high-

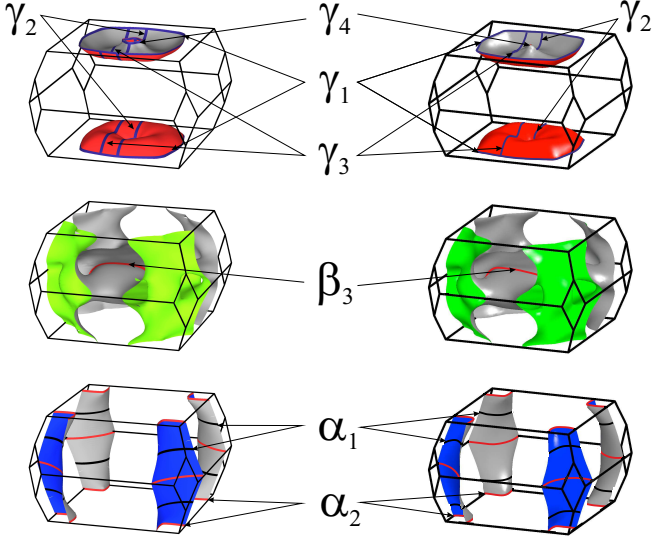


FIG. 3: (Color online) Fermi surface of LaFe_2P_2 calculated using the ABINIT code (left) and the FPLO code applying the LDA+ U approach (right). The upper Fermi-surface sheet is hole-like, the other two electron-like. Solid lines mark extremal orbits.

field data [Fig. 1(b)], two additional dHvA orbits appear, with frequencies $F_{\gamma_4} \approx 370$ T and $F_{\gamma_1} = 9320(30)$ T, besides the harmonics of F_{α_1} and F_{α_2} . The experimentally observed dHvA frequencies as a function of the angles Θ_{010} (rotation from c to a) and Θ_{001} (in-plane rotation) are shown in Fig. 2(a) together with data obtained from the band structure calculated using the ABINIT code.

From the seven independent dHvA frequencies, some could only be observed at the higher magnetic fields available in Grenoble [open symbols in Fig. 2(a)]. Dominant are the dHvA signals labeled α_1 and α_2 (Fig. 1) [27]. The average of these frequencies follows a $1/\cos(\Theta)$ dependence [dashed line in Fig. 2(a)] indicative of a corrugated quasi-two-dimensional Fermi surface. Such a warped Fermi-surface cylinder leads to a peculiar well-defined angular dependence of the dHvA frequencies and amplitudes. At the so-called Yamaji angle [28], the point at which the two dHvA frequencies merge, at about 25° , a strong enhancement of the dHvA amplitude is expected, since effectively the extremal Fermi-surface area along the applied-field direction stays constant – as for an ideally two-dimensional metal – meaning that all electrons on that Fermi-surface sheet contribute to the dHvA signal. This, indeed, fits nicely with the experimental observation as shown in Fig. 2(b).

In order to assign the observed dHvA frequencies to extremal Fermi-surface orbits, we performed comprehensive band-structure calculations, as described above. Using the FPLO code (applying the LDA+ U approach to the La $4f$ states) the resulting Fermi surfaces together with the most prominent extremal orbits for fields along $[001]$ are shown in the right part of Fig. 3. We obtain a very sim-

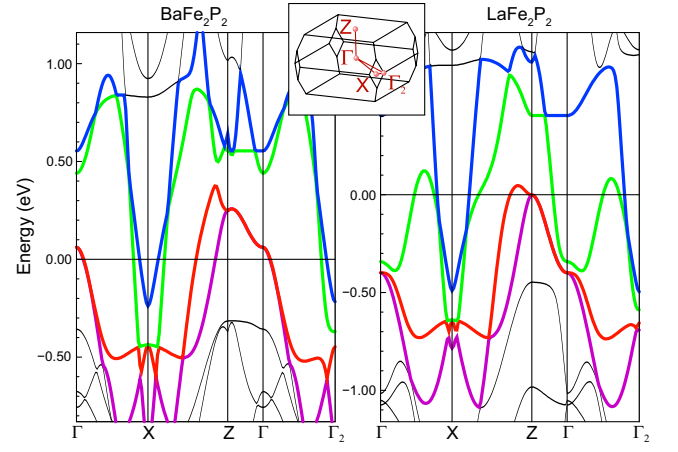


FIG. 4: (Color online) Band structure of BaFe_2P_2 (left) and LaFe_2P_2 (right) calculated using the FPLO code. The Fermi energy in the right panel is shifted by about 0.3 eV visualizing the additional band filling caused by the trivalent La ions. The inset shows the Brillouin zone with symmetry points.

ilar Fermi-surface topology when using the ABINIT code, shown in the left part of Fig. 3. Our calculated Fermi surface more or less agrees with the recently published one in Ref. 29, but shows some significant differences to the one reported in Ref. 25.

From the angular dependence of the extremal orbits the dHvA frequencies were calculated. The result using the ABINIT code is shown by solid lines in Fig. 2(a). As a robust feature in all our band-structure calculations, we find a strongly corrugated cylinder at the Brillouin-zone corner, i.e., at the X point (lower row in Fig. 3). Such a cylinder is well known for the iron pnictides. There is, however, no hole-like cylinder at the zone center Γ . Therefore, the usually realized, at least partial, nesting between a cylinder at Γ and one at X is absent – and the electron pairing, essential to the s_{\pm} model [1–4], is not possible. Instead of a cylinder, a donut-shaped hole-like Fermi surface appears near Z and a complicated “monster” fills more or less the whole Brillouin zone.

Although mainly minor, some differences in the Fermi-surface topologies are found when using the ABINIT or FPLO code. With the former, the hole of the donut is somewhat larger, fitting perfectly to the experimental data [γ_4 orbit in Fig. 2(a)]. On the other hand, the α orbits of the cylinder at X calculated using FPLO are about 7% smaller than in the ABINIT code and fit the data better. It is worth noting that the area of the cylinder depends strongly on the distance between the FeP planes which would explain the slightly enhanced theoretical dHvA frequencies. Anyway, the agreement between experiment and our band-structure calculations is very good [Fig. 2(a)]. For the cylinder at X , the calculations predict crossings of the α_1 and α_2 orbits exactly

at the experimentally observed angles. Close to [001], we observe dHvA signals near 10 kT that can be assigned to the γ_1 orbit of the donut. The dHvA frequencies which are appearing at about 3000 T for a Θ_{010} above 50° can be assigned as well to the γ_3 donut as to an orbit of the multi-branched β surface (this β orbit is not visible in the visualization shown in Fig. 3). For Θ_{010} between about 49° and 83° (Fig. 2), we could resolve the β_3 orbit of the multi-branched Fermi surface which is nicely in line with the calculations. Some of the predicted β orbits appearing over narrow angular ranges [gray lines in Fig. 2(a)] have not been observed experimentally.

For comparison, we also performed band-structure calculations for LaFe_2As_2 and BaFe_2P_2 . In the first case, the Fermi surface is almost unchanged which indicates that the Γ hole-like cylinder is destroyed by replacing Ba with La and not by the substitution of As by P. Our results for BaFe_2P_2 are in agreement with those found in the literature [30] with a hole-like cylinder in the zone center. In Fig. 4, we show the band-structure dispersions for BaFe_2P_2 (left) and LaFe_2P_2 (right). The bands crossing the Fermi energy are highlighted by bold colored lines corresponding to the coloring of the Fermi surfaces in Fig. 3. The overall dispersions of these bands is similar for both compounds. Although there are some clear differences in the dispersions of the bands, the major effect is an upward shift of the Fermi energy in LaFe_2P_2 . This can be easily explained by the presence of the trivalent La adding an additional electron to the Fermi sea, filling up the bands to a higher level. As a second effect for a change of the Fermi surface, we observe a surprisingly strong hybridization of the La $5d$ electrons with the Fe $3d$ and the P $3p$ states. In contrast, Ba states essentially do not contribute to the states near the Fermi level in BaFe_2P_2 . In consequence, the hole-like cylinders around Γ in BaFe_2P_2 originating in the red and magenta bands disappear in LaFe_2P_2 (Fig. 4). In addition, only one electron-like cylinder around X remains for LaFe_2P_2 .

From the temperature dependence of the dHvA oscillation amplitudes we determined the effective masses, as summarized in Table I. We find substantially smaller masses for the α orbits than reported previously [25]. Anyhow, when comparing with the calculated masses (using the FPLO code) [31], our experimental results show that there exist considerable mass renormalizations for all bands. These enhanced values are in agreement with the strong correlations expected in the model where a Kondo-like exchange mechanism is used to describe the dual nature of the iron d electrons, being at the same time localized and itinerant [6, 7].

When extracting the mass-enhancement factors, $\lambda = m/m_b - 1$, from the calculated, m_b , and measured, m , masses, we obtain values for λ between 1.2 and 2.2 for the different bands. For other 122 materials such strong many-body correlations are sufficient for superconductivity to occur [12]. This strongly suggests that the absence

TABLE I: Comparison between the calculated (using the FPLO code) and measured dHvA frequencies and effective masses for different bands and field orientations in LaFe_2P_2 .

Θ_{010}	orbit	measured		calculated	
		$F(\text{T})$	m/m_e	$F(\text{T})$	m_b/m_e
0°	α_1	2570	1.5(1)	2730	0.68
0°	α_2	3110	1.7(1)	3350	0.70
75°	γ_3	2880	3.1(1)	3100	0.98
75°	β_3	6510	3.6(2)	6110	1.53

of the hole-like cylinder around Γ indeed prevents the material from becoming a superconductor. Our results indicate that both sufficient nesting and strong many-body interactions are needed for the appearance of superconductivity, most probably of the extended s -wave type. However, more detailed models are needed to elucidate which mass renormalization correlates with the pairing potential.

In conclusion, our dHvA data combined with band-structure calculations allowed to reveal a detailed picture of the Fermi-surface topology of LaFe_2P_2 . Compared to other 122 pnictides, the electron-like Fermi-surface cylinder in the Brillouin-zone corner persists, whereas the hole-like cylinder is absent. Instead a donut-like and a multi-branched Fermi-surface sheet emerge. In spite of strong mass renormalizations, ascribed to Kondo-like electronic correlations, no superconductivity is found which can be explained by the absence of sufficient nesting between the electron and hole parts of the Fermi surface.

The research at UdeM received support from the Natural Sciences and Engineering Research Council of Canada (Canada), Fonds Québécois de la Recherche sur la Nature et les Technologies (Québec), and the Canada Research Chair Foundation. Computational resources were provided by Calcul Québec and Compute Canada. Z.F. acknowledges Grant No. NSF-DMR-0503361. Part of this work was supported by EuroMagNET II (EU contract No. 228043) and by the Deutsche Forschungsgemeinschaft (SPP 1458).

* Current address: Laboratory for Developments and Methods, Paul Scherrer Institute, CH-5232 Villigen, Switzerland

- [1] I. I. Mazin, D. J. Singh, M. D. Johannes, and M. H. Du, Phys. Rev. Lett. **101**, 057003 (2008).
- [2] M. M. Korshunov and I. Eremin, Phys. Rev. B **78**, 140509(R) (2008).
- [3] V. Cvetkovic and Z. Tesanovic, EPL **85**, 37002 (2009).
- [4] I. I. Mazin, Nature (London) **464**, 183 (2010).
- [5] Q. Si and E. Abrahams, Phys. Rev. Lett. **101**, 076401 (2008).

- [6] P. Dai, J. Hu, and E. Dagotto, *Nat. Phys.* **8**, 709 (2012).
- [7] L. P. Gor'kov, and G. B. Teitel'baum, *Phys. Rev. B* **87**, 024504 (2013).
- [8] B. Bergk, V. Petzold, H. Rosner, S.-L. Drechsler, M. Bartkowiak, O. Ignatchik, A. D. Bianchi, I. Sheikin, P. C. Canfield, and J. Wosnitzer, *Phys. Rev. Lett.* **100**, 257004 (2008).
- [9] S. E. Sebastian, J. Gillett, N. Harrison, P. H. C. Lau, D. J. Singh, C. H. Mielke, and G. G. Lonzarich, *J. Phys.: Condens. Matter* **20**, 422203 (2008).
- [10] J. G. Analytis, R. D. McDonald, J.-H. Chu, S. C. Riggs, A. F. Bangura, C. Kucharczyk, M. Johannes, and I. R. Fisher, *Phys. Rev. B* **80**, 064507 (2009).
- [11] N. Harrison, R. D. McDonald, C. H. Mielke, E. D. Bauer, F. Ronning, and J. D. Thompson, *J. Phys.: Condens. Matter* **21**, 322202 (2009).
- [12] A. Carrington, *Rep. Prog. Phys.* **74**, 124507 (2011).
- [13] A. I. Coldea, D. Braithwaite, and A. Carrington, *C. R. Physique* **14**, 94 (2013).
- [14] S. R. Saha, N. P. Butch, T. Drye, J. Magill, S. Ziemak, K. Kirshenbaum, P. Y. Zavalij, J. W. Lynn, and J. Paglione, *Phys. Rev. B* **85**, 024525 (2012).
- [15] E. Mörsen, B. D. Mosel, W. Müller-Warmuth, M. Reehuis, and W. Jeitschko, *J. Phys. Chem. Solids* **49**, 785 (1988).
- [16] M. Reehuis and W. Jeitschko, *J. Phys. Chem. Solids* **51**, 961 (1990).
- [17] For example, the appearance of the hole in the donut-shaped Fermi surface depends on the exact positions of the P atoms.
- [18] K. Koepernik and H. Eschrig, *Phys. Rev. B* **59**, 1743 (1999).
- [19] J. P. Perdew and Y. Wang, *Phys. Rev. B* **45**, 13244 (1992).
- [20] J. P. Perdew, K. Burke, and M. Ernzerhof, *Phys. Rev. Lett.* **77**, 3865 (1996).
- [21] The P atom position was relaxed from $z = 0.3555$, the experimental value of the z position, to $z = 0.3477$.
- [22] In consequence of this unphysical energy position of the $4f$ states, the Fermi surface may easily be distorted due to their hybridization with the conduction electrons.
- [23] In order to safely shift the La $4f$ states away from the Fermi energy we arbitrarily chose $U = 8$ eV.
- [24] X. Gonze, B. Amadon, P.-M. Anglade, J.-M. Beuken, F. Bottin, P. Boulanger, F. Bruneval, D. Caliste, R. Caracas, M. Côté, et al., *Comput. Phys. Commun.* **180**, 2582 (2009).
- [25] H. Muranaka, Y. Doi, K. Katayama, H. Sugawara, R. Settai, F. Honda, T. D. Matsuda, Y. Haga, H. Yamagami, and Y. Onuki, *J. Phys. Soc. Jpn.* **78**, 053705 (2009).
- [26] We estimate the uncertainty in the correct sample alignment to be about 2° .
- [27] For some angles a third peak in the Fourier transformation appeared next to the other α frequencies that most probably originates in another extremal area of the strongly corrugated Fermi-surface cylinder.
- [28] K. Yamaji, *J. Phys. Soc. Jpn.* **58**, 1520 (1989).
- [29] P. J. W. Moll, J. Kanter, R. D. McDonald, F. Balakirev, P. Blaha, K. Schwarz, Z. Bukowski, N. D. Zhigadlo, S. Katrych, K. Mattenberger, J. Karpinski, and B. Batlogg, *Phys. Rev. B* **84**, 224507 (2011).
- [30] H. Shishido, A. F. Bangura, A. I. Coldea, S. Tonegawa, K. Hashimoto, S. Kasahara, P. M. C. Rourke, H. Ikeda, T. Terashima, R. Settai, et al., *Phys. Rev. Lett.* **104**, 057008 (2010).
- [31] The calculated masses are very similar when using either the FPLO or ABINIT code.